

## Measurement of the $e^+e^- \rightarrow D^{(*)+}D^{(*)-}$ cross sections

T. Uglov,<sup>10</sup> K. Abe,<sup>6</sup> K. Abe,<sup>37</sup> T. Abe,<sup>6</sup> H. Aihara,<sup>39</sup> M. Akatsu,<sup>18</sup> Y. Asano,<sup>43</sup> T. Aso,<sup>42</sup> V. Aulchenko,<sup>1</sup> A. M. Bakich,<sup>34</sup> Y. Ban,<sup>28</sup> U. Bitenc,<sup>11</sup> I. Bizjak,<sup>11</sup> A. Bondar,<sup>1</sup> A. Bozek,<sup>22</sup> M. Bračko,<sup>17,11</sup> T. E. Browder,<sup>5</sup> Y. Chao,<sup>21</sup> B. G. Cheon,<sup>33</sup> R. Chistov,<sup>10</sup> S.-K. Choi,<sup>4</sup> Y. Choi,<sup>33</sup> A. Chuvikov,<sup>29</sup> S. Cole,<sup>34</sup> M. Danilov,<sup>10</sup> A. Drutskoy,<sup>10</sup> S. Eidelman,<sup>1</sup> V. Eiges,<sup>10</sup> Y. Enari,<sup>18</sup> D. Epifanov,<sup>1</sup> S. Fratina,<sup>11</sup> N. Gabyshev,<sup>6</sup> A. Garmash,<sup>29</sup> T. Gershon,<sup>6</sup> B. Golob,<sup>16,11</sup> N. C. Hastings,<sup>6</sup> H. Hayashii,<sup>19</sup> M. Hazumi,<sup>6</sup> T. Hokuue,<sup>18</sup> Y. Hoshi,<sup>37</sup> H.-C. Huang,<sup>21</sup> K. Inami,<sup>18</sup> A. Ishikawa,<sup>6</sup> H. Iwasaki,<sup>6</sup> M. Iwasaki,<sup>39</sup> Y. Iwasaki,<sup>6</sup> J. H. Kang,<sup>46</sup> J. S. Kang,<sup>13</sup> P. Kapusta,<sup>22</sup> N. Katayama,<sup>6</sup> H. Kawai,<sup>2</sup> T. Kawasaki,<sup>24</sup> H. Kichimi,<sup>6</sup> H. J. Kim,<sup>46</sup> J. H. Kim,<sup>33</sup> S. K. Kim,<sup>32</sup> K. Kinoshita,<sup>47</sup> P. Koppenburg,<sup>6</sup> S. Korpar,<sup>17,11</sup> P. Krokovny,<sup>1</sup> S. Kumar,<sup>27</sup> A. Kuzmin,<sup>1</sup> Y.-J. Kwon,<sup>46</sup> J. S. Lange,<sup>3,30</sup> G. Leder,<sup>9</sup> S. H. Lee,<sup>32</sup> T. Lesiak,<sup>22</sup> J. Li,<sup>31</sup> S.-W. Lin,<sup>21</sup> D. Liventsev,<sup>10</sup> J. MacNaughton,<sup>9</sup> G. Majumder,<sup>35</sup> H. Matsumoto,<sup>24</sup> T. Matsumoto,<sup>40</sup> A. Matyja,<sup>22</sup> W. Mitaroff,<sup>9</sup> H. Miyake,<sup>26</sup> H. Miyata,<sup>24</sup> D. Mohapatra,<sup>44</sup> T. Nagamine,<sup>38</sup> Y. Nagasaka,<sup>7</sup> T. Nakadaira,<sup>39</sup> E. Nakano,<sup>25</sup> M. Nakao,<sup>6</sup> S. Nishida,<sup>6</sup> O. Nitoh,<sup>41</sup> T. Nozaki,<sup>6</sup> S. Ogawa,<sup>36</sup> T. Ohshima,<sup>18</sup> S. Okuno,<sup>12</sup> S. L. Olsen,<sup>5</sup> W. Ostrowicz,<sup>22</sup> H. Ozaki,<sup>6</sup> P. Pakhlov,<sup>10</sup> H. Palka,<sup>22</sup> C. W. Park,<sup>13</sup> H. Park,<sup>14</sup> N. Parslow,<sup>34</sup> L. S. Peak,<sup>34</sup> L. E. Piiilonen,<sup>44</sup> Y. Sakai,<sup>6</sup> O. Schneider,<sup>15</sup> J. Schümann,<sup>21</sup> C. Schwanda,<sup>9</sup> S. Semenov,<sup>10</sup> K. Senyo,<sup>18</sup> R. Seuster,<sup>5</sup> H. Shibuya,<sup>36</sup> B. Shwartz,<sup>1</sup> V. Sidorov,<sup>1</sup> J. B. Singh,<sup>27</sup> N. Soni,<sup>27</sup> R. Stamen,<sup>6</sup> S. Stanič,<sup>43,\*</sup> M. Starič,<sup>11</sup> T. Sumiyoshi,<sup>40</sup> S. Suzuki,<sup>45</sup> O. Tajima,<sup>38</sup> F. Takasaki,<sup>6</sup> K. Tamai,<sup>6</sup> N. Tamura,<sup>24</sup> M. Tanaka,<sup>6</sup> Y. Teramoto,<sup>25</sup> T. Tomura,<sup>39</sup> T. Tsuboyama,<sup>6</sup> T. Tsukamoto,<sup>6</sup> S. Uehara,<sup>6</sup> Y. Unno,<sup>2</sup> S. Uno,<sup>6</sup> G. Varner,<sup>5</sup> K. E. Varvell,<sup>34</sup> C. C. Wang,<sup>21</sup> C. H. Wang,<sup>20</sup> L. Widhalm,<sup>9</sup> B. D. Yabsley,<sup>44</sup> Y. Yamada,<sup>6</sup> A. Yamaguchi,<sup>38</sup> Y. Yamashita,<sup>23</sup> M. Yamauchi,<sup>6</sup> Heyoung Yang,<sup>32</sup> J. Ying,<sup>28</sup> Y. Yusa,<sup>38</sup> C. C. Zhang,<sup>8</sup> V. Zhilich,<sup>1</sup> and D. Žontar<sup>16,11</sup>

(Belle Collaboration)

<sup>1</sup>*Budker Institute of Nuclear Physics, Novosibirsk*

<sup>2</sup>*Chiba University, Chiba*

<sup>3</sup>*University of Frankfurt, Frankfurt*

<sup>4</sup>*Gyeongsang National University, Chinju*

<sup>5</sup>*University of Hawaii, Honolulu, Hawaii 96822, USA*

<sup>6</sup>*High Energy Accelerator Research Organization (KEK), Tsukuba*

<sup>7</sup>*Hiroshima Institute of Technology, Hiroshima*

<sup>8</sup>*Institute of High Energy Physics, Chinese Academy of Sciences, Beijing*

<sup>9</sup>*Institute of High Energy Physics, Vienna*

<sup>10</sup>*Institute for Theoretical and Experimental Physics, Moscow*

<sup>11</sup>*J. Stefan Institute, Ljubljana*

<sup>12</sup>*Kanagawa University, Yokohama*

<sup>13</sup>*Korea University, Seoul*

<sup>14</sup>*Kyungpook National University, Taegu*

<sup>15</sup>*Swiss Federal Institute of Technology of Lausanne, EPFL, Lausanne*

<sup>16</sup>*University of Ljubljana, Ljubljana*

<sup>17</sup>*University of Maribor, Maribor*

<sup>18</sup>*Nagoya University, Nagoya*

<sup>19</sup>*Nara Women's University, Nara*

<sup>20</sup>*National United University, Miao Li*

<sup>21</sup>*Department of Physics, National Taiwan University, Taipei*

<sup>22</sup>*H. Niewodniczanski Institute of Nuclear Physics, Krakow*

<sup>23</sup>*Nihon Dental College, Niigata*

<sup>24</sup>*Niigata University, Niigata*

<sup>25</sup>*Osaka City University, Osaka*

<sup>26</sup>*Osaka University, Osaka*

<sup>27</sup>*Panjab University, Chandigarh*

<sup>28</sup>*Peking University, Beijing*

<sup>29</sup>*Princeton University, Princeton, New Jersey 08545, USA*

<sup>30</sup>*RIKEN BNL Research Center, Upton, New York 11973, USA*

<sup>31</sup>*University of Science and Technology of China, Hefei*

<sup>32</sup>*Seoul National University, Seoul*

<sup>33</sup>*Sungkyunkwan University, Suwon*

<sup>34</sup>*University of Sydney, Sydney NSW*

<sup>35</sup>*Tata Institute of Fundamental Research, Bombay*<sup>36</sup>*Toho University, Funabashi*<sup>37</sup>*Tohoku Gakuin University, Tagajo*<sup>38</sup>*Tohoku University, Sendai*<sup>39</sup>*Department of Physics, University of Tokyo, Tokyo*<sup>40</sup>*Tokyo Metropolitan University, Tokyo*<sup>41</sup>*Tokyo University of Agriculture and Technology, Tokyo*<sup>42</sup>*Toyama National College of Maritime Technology, Toyama*<sup>43</sup>*University of Tsukuba, Tsukuba*<sup>44</sup>*Virginia Polytechnic Institute and State University, Blacksburg, Virginia 24061, USA*<sup>45</sup>*Yokkaichi University, Yokkaichi*<sup>46</sup>*Yonsei University, Seoul*<sup>47</sup>*University of Cincinnati, Cincinnati, Ohio 45221, USA*

(Received 29 January 2004; published 20 October 2004)

We report first measurements of  $e^+e^- \rightarrow D^{(*)+}D^{(*)-}$  processes far above threshold. The cross sections for  $e^+e^- \rightarrow D_T^{*+}D_L^{*-}$  and  $e^+e^- \rightarrow D^+D_T^{*-}$  at  $\sqrt{s} \simeq 10.6$  GeV/ $c^2$  are measured to be  $0.55 \pm 0.03 \pm 0.05$  and  $0.62 \pm 0.03 \pm 0.06$  pb, respectively. We set upper limits on the cross sections for  $e^+e^- \rightarrow D_T^{*+}D_T^{*-}$ ,  $e^+e^- \rightarrow D_L^{*+}D_L^{*-}$ ,  $e^+e^- \rightarrow D^+D_L^{*-}$ , and  $e^+e^- \rightarrow D^+D^-$  processes. The analysis is based on  $88.9$  fb $^{-1}$  of data collected by the Belle experiment at the KEKB  $e^+e^-$  asymmetric collider.

DOI: 10.1103/PhysRevD.70.071101

PACS numbers: 13.66.Bc, 12.39.Hg, 13.87.Fh

The processes  $e^+e^- \rightarrow D^{(*)}\bar{D}^{(*)}$ , with no extra fragmentation particles in the final state, have not previously been measured for energies  $\sqrt{s} \gg 2M_D$ . The cross sections for these processes can be computed once the charmed meson form factors are determined for the appropriate value of momentum transfer,  $q^2 \equiv s$ . In the Heavy Quark Effective Theory approach based on heavy-quark spin symmetry, the form factors can be expressed in terms of a universal form factor, the Isgur-Wise function. With rising  $q^2$  the leading-twist contribution, which violates heavy-quark spin symmetry, also becomes important. A calculation that takes these effects into account [1] predicts that the cross sections for  $e^+e^- \rightarrow D\bar{D}^*$  and  $D_L^*\bar{D}_T^*$  are equal; cross sections for  $D_L^*\bar{D}_L^*$  and  $D_T^*\bar{D}_T^*$  are expected to be suppressed by factors  $\sim 20$  and  $30$  at  $\sqrt{s} \simeq 10.6$  GeV, and that for  $e^+e^- \rightarrow D\bar{D}$  by a factor  $\sim 10^3$ . (Subscripts indicate longitudinal  $L$  and transverse  $T$  polarizations of the  $D^*$ ). The prediction for the scale of the cross sections  $\sigma(e^+e^- \rightarrow D_L^*\bar{D}_T^*) \simeq 2.5$  pb is uncertain by a factor  $\sim 3$ , because the theoretical formulas contain poorly known parameters, while the prediction of ratios is expected to be more robust [2]. Recently, new calculations in the framework of the constituent quark model have become available [3], which differ from the predictions of [1] in both absolute and relative cross sections. The observation of  $e^+e^- \rightarrow D^{(*)}\bar{D}^{(*)}$  processes leads to the possibility of double tag studies at  $\sqrt{s} \sim 10.6$  GeV. These studies were previously possible only at resonances such as the  $\psi(3.77)$  in the 3–4 GeV energy range.

In this paper, we present the first measurement of the  $e^+e^- \rightarrow D^{*+}D^{*-}$  and  $e^+e^- \rightarrow D^+D^{*-}$  [4] cross sections and polarizations at  $\sqrt{s} \simeq 10.6$  GeV. We also set an upper limit on the cross section for  $e^+e^- \rightarrow D^+D^-$ . The present

study is limited to final states that contain charged  $D^{(*)}$  mesons only. Since the contribution of the electromagnetic current coupled to light quarks is negligible compared to that for heavy quarks, the neutral and charged charm meson cross sections are expected to be the same [1].

The analysis is based on  $88.9$  fb $^{-1}$  of data at the  $Y(4S)$  resonance and nearby continuum, collected with the Belle detector [5] at the KEKB asymmetric energy  $e^+e^-$  collider [6]. We select well-reconstructed tracks consistent with originating from the interaction region as charged pion candidates. Those passing particle identification cuts based on  $dE/dx$ , aerogel Čerenkov, and time-of-flight information [5] are selected as charged kaon candidates. We then reconstruct  $D^0$  and  $D^+$  mesons in the decay modes  $D^0 \rightarrow K^-\pi^+$ ,  $D^0 \rightarrow K^-\pi^+\pi^+\pi^-$ , and  $D^+ \rightarrow K^-\pi^+\pi^+$ . The selected combinations are constrained to a common vertex, and quality cuts are imposed on the vertex fit to reduce the combinatorial background. A 15 MeV/ $c^2$  interval around the nominal  $D$  masses is used to select  $D^0 \rightarrow K^-\pi^+$  and  $D^+ \rightarrow K^-\pi^+\pi^+$  candidates; for the  $D^0 \rightarrow K^-\pi^+\pi^+\pi^-$  decay mode, the signal window is chosen to be 10 MeV/ $c^2$  around the nominal  $D^0$  mass ( $\sim 2\sigma$  in each case). The selected  $D$  candidates are then subjected to a mass and vertex constrained fit to improve their momentum resolution. The  $D^{*+}$  mesons are reconstructed in the  $D^0\pi^+$  decay mode. The mass of the  $D^0\pi^+$  combination is required to be within a 2 MeV/ $c^2$  ( $\sim 3\sigma$ ) mass interval around the nominal  $D^{*+}$  mass.

The processes  $e^+e^- \rightarrow D^{(*)+}D^{(*)-}$  can be identified by energy-momentum balance in fully reconstructed events that contain only a pair of charm mesons. However, the small charm meson reconstruction efficiency of the studied channels results in a tiny total efficiency in this case [the typical efficiency including the intermediate

\*On leave from Nova Gorica Polytechnic, Nova Gorica.

branching fractions is (0.01–0.1)% depending on the final state]. Because of the simple two-body kinematics, it is sufficient to reconstruct only one of the two charmed mesons in the event to identify the processes of interest. For simplicity, we refer to the fully reconstructed  $D$  meson as the  $D^{(*)+}$ , and the other as the  $D^{*-}$ . We choose the mass of the system recoiling against the reconstructed  $D^{(*)+}$  [ $M_{\text{recoil}}(D^{(*)+})$ ] as a discriminating variable:  $M_{\text{recoil}}(D^{(*)+}) = \sqrt{(\sqrt{s} - E_{D^{(*)+}})^2 - \vec{p}_{D^{(*)+}}^2}$ , where  $\sqrt{s}$  is the total center-of mass (c.m.) energy, and  $E_{D^{(*)+}}$  and  $\vec{p}_{D^{(*)+}}$  are the c.m. energy and momentum of the reconstructed  $D^{(*)+}$ . For the signal, a peak in the  $M_{\text{recoil}}$  distribution around the nominal  $D^-$  or  $D^{*-}$  mass is expected. This method increases the efficiency by a factor of 30–100, compared to full event reconstruction, but suffers from higher background. For the  $e^+e^- \rightarrow D^+D^{*-}$  and  $e^+e^- \rightarrow D^{*+}D^{*-}$  processes, we find a better compromise between higher statistics and smaller background: The first  $D^{(*)+}$  is fully reconstructed, while the recoiling  $D^{*-}$  is required to decay into  $\bar{D}^0\pi_{\text{slow}}^-$ . The reconstructed  $\pi_{\text{slow}}^-$  provides extra information that allows us to reduce the background to a negligible level using the difference between the masses of the systems recoiling against the  $D^{(*)+}\pi_{\text{slow}}^-$  combination, and against the  $D^{(*)+}$  alone,  $\Delta M_{\text{recoil}} \equiv M_{\text{recoil}}(D^{(*)+}) - M_{\text{recoil}}(D^{(*)+}\pi_{\text{slow}}^-)$ . The variable  $\Delta M_{\text{recoil}}$  peaks around the nominal  $D^{*-} - \bar{D}^0$  mass difference with a resolution of  $\sigma_{\Delta M_{\text{recoil}}} \sim 1 \text{ MeV}/c^2$  as found by Monte Carlo (MC) simulation. For  $e^+e^- \rightarrow D^{*+}D^{*-}$  and  $e^+e^- \rightarrow D^+D^{*-}$ , we require  $\Delta M_{\text{recoil}}$  to be within a  $\pm 2 \text{ MeV}/c^2$  interval around the nominal  $M_{D^{*-}} - M_{\bar{D}^0}$  mass difference. The last method allows one to reduce the background down to a negligible level as will be shown below at the expense of the factor of 3 smaller efficiency.

The  $M_{\text{recoil}}(D^{*+})$  and  $M_{\text{recoil}}(D^+)$  distributions are shown in Figs. 1(a) and 1(b), respectively. Clear signals are seen around the nominal  $D^{*-}$  mass in both cases. The higher recoil mass tails in the signal distributions are due to initial state radiation (ISR). The  $M_{\text{recoil}}$  distributions for events in the  $\Delta M_{\text{recoil}}$  sideband ( $0.150 \text{ MeV}/c^2 < \Delta M_{\text{recoil}} < 0.154 \text{ MeV}/c^2$ ) are shown as the hatched histogram [barely visible in Fig. 1(a) due to its small size].

The backgrounds in the region  $M_{\text{recoil}} < 2.1 \text{ GeV}/c^2$  are negligible for both processes, so we consider this interval as the signal region. There are three possible background sources:

- (i) incorrectly reconstructed  $D^{*+}$  or  $D^+$ ;
- (ii)  $e^+e^- \rightarrow D^{(*)+}Dn\pi^-$  ( $n \geq 0$ ), where the  $\pi_{\text{slow}}^-$  is not produced from  $D^{*-}$  decay (and can be either from fragmentation or from unreconstructed  $D$  decay), and thus produces no peak in the  $\Delta M_{\text{recoil}}$  distribution;
- (iii)  $e^+e^- \rightarrow D^{(*)+}D^{*-}n\pi$ , where  $n \geq 1$ .

First we consider the process  $e^+e^- \rightarrow D^{*+}D^{*-}$ . To estimate background (i) numerically, we count the entries in

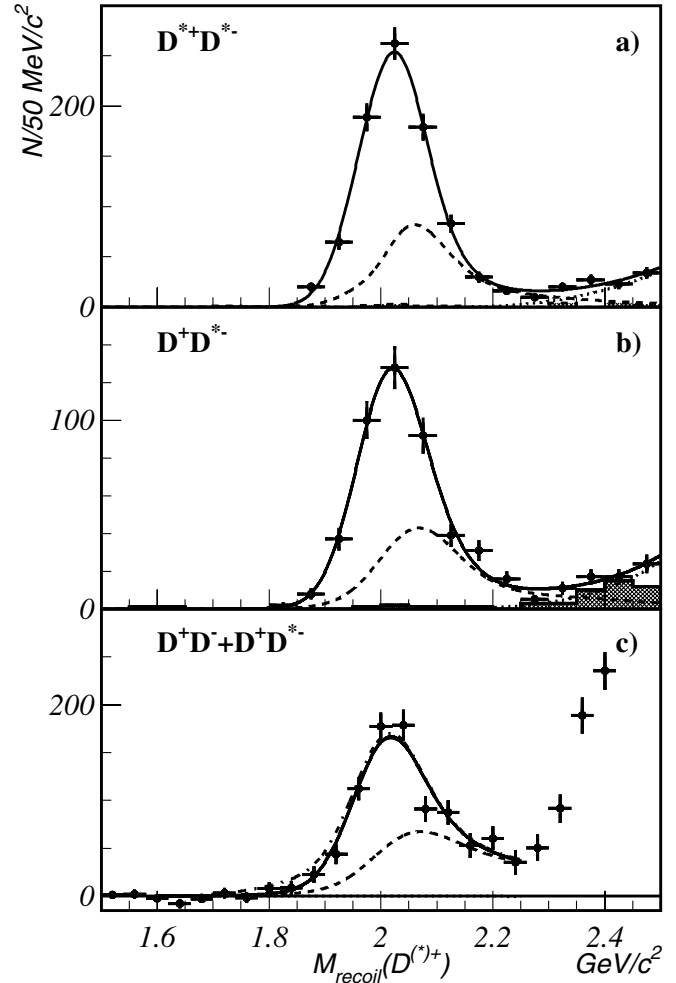


FIG. 1. (a)  $M_{\text{recoil}}(D^{*+})$  and (b)  $M_{\text{recoil}}(D^+)$  after applying the  $\Delta M_{\text{recoil}}$  requirement. Points show the  $\Delta M_{\text{recoil}}$  signal region; hatched histograms show the  $\Delta M_{\text{recoil}}$  sideband; solid lines represent the fits described in the text; dashed lines show the contribution due to events with ISR photons of significant energy; dotted lines are the expected background contribution. (c)  $M_{\text{recoil}}(D^+)$  after  $D^+$  sideband subtraction without requiring an extra  $\pi_{\text{slow}}^-$  in the event.

the signal region for  $D^0\pi^+$  combinations taken from the  $D^{*+}$  mass sideband ( $2.016 \text{ GeV}/c^2 < M_{D^0\pi^+} < 2.020 \text{ GeV}/c^2$ ). Three events are found in the data, while the MC predicts a contribution of 2.5 events from the signal process due to non-Gaussian tails in the  $M_{D^{*+}}$  resolution function. The signal MC is normalized to the number of entries in the  $M_{\text{recoil}}(D^{*+}) < 2.1 \text{ GeV}/c^2$  region in the data. Background (ii) is estimated using the  $\Delta M_{\text{recoil}}$  sideband ( $0.150 \text{ MeV}/c^2 < \Delta M_{\text{recoil}} < 0.154 \text{ MeV}/c^2$ ). In the signal region eight events are found; four events are expected according to MC from the signal process because of significant energy ISR. Thus, the upper limits for the extra backgrounds (i) and (ii) which are not related to the signal events are estimated to be smaller than five and ten events at the 90% C.L., respectively [7]. The remaining background (iii) can result in peaks in both the  $M(D^{*+})$  and  $\Delta M_{\text{recoil}}$  distribu-

tions, but has a threshold in the  $M_{\text{recoil}}$  distribution at  $M_{D^{*+}} + M_{\pi^0} = 2.15 \text{ GeV}/c^2$ , which is  $\sim 1\sigma$  higher than the chosen  $M_{\text{recoil}}$  signal interval. To estimate the residual background (iii) contribution in the signal region, we perform a fit to the  $M_{\text{recoil}}(D^{*+})$  distribution. The signal function is determined from the MC simulation and parametrized as the sum of a core Gaussian and an asymmetric function representing the case when the studied process is accompanied by radiative photon(s) with significant energy ( $E_{\text{ISR}} > 10 \text{ MeV}$ ). The  $M_{\text{recoil}}(D^{*+})$  resolution due to detector smearing and the signal function offset are left as free parameters in the fit to check the agreement with the MC predictions. The background (iii) distribution is parametrized by a threshold function,  $\alpha[M_{\text{recoil}}(D^{*+}) - M(D^{*-}) - M(\pi^0)]^\beta$ , convolved with the detector resolution, where  $\alpha$  and  $\beta$  are free parameters. The fit results are shown in Fig. 1(a) as a solid curve; the dashed line shows the contribution of the studied process with significant energy ISR photons ( $E_{\text{ISR}} > 10 \text{ MeV}$ ). The dotted line represents the expected background (iii) distribution. The signal yield is found to be  $815 \pm 29$  events in the whole fit region ( $676 \pm 26$  events in the signal region  $M_{\text{recoil}} < 2.1 \text{ GeV}/c^2$ ). The  $M_{\text{recoil}}$  resolution  $\sigma = 56.1 \pm 2.2 \text{ MeV}/c^2$  is found to be in excellent agreement with the MC expectation ( $56.4 \text{ MeV}/c^2$ ), and the shift of the signal peak position in the data with respect to the MC position is found to be consistent with zero ( $0.6 \pm 2.5 \text{ MeV}/c^2$ ). The contribution from background (iii) in the signal region is estimated from this fit to be less than two events at the 90% C.L.

For the process  $e^+e^- \rightarrow D^+D^{*-}$ , proceeding in a similar way, we find a signal yield of  $423 \pm 21$  events in the whole fit region ( $360 \pm 19$  events in the signal region  $M_{\text{recoil}} < 2.1 \text{ GeV}/c^2$ ), with backgrounds (i), (ii), and (iii) smaller than eight, six, and two events at the 90% C.L., respectively. Finally, we estimate the total background in the  $M_{\text{recoil}} < 2.1 \text{ GeV}/c^2$  interval to be smaller than 13 and ten events for the  $e^+e^- \rightarrow D^{*+}D^{*-}$  and  $e^+e^- \rightarrow D^+D^{*-}$  processes, respectively, which is of the order of 1% of the signal. We therefore assume that all events in the interval  $M_{\text{recoil}} < 2.1 \text{ GeV}/c^2$  are signal, and include the possible background contribution in the systematic error.

Since the reconstruction efficiency depends on the production and  $D^{*\pm}$  helicity angle distributions, we perform an angular analysis before computing cross sections. The helicity angle is defined as an angle between  $D^0$  momentum in the  $D^*$  rest frame and the  $D^*$  direction in the center-of-mass frame and is calculated for the nonreconstructed  $D^{*-}$  assuming two-body kinematics. A scatter plot of the helicity angles for the two  $D^*$  mesons from  $e^+e^- \rightarrow D^{*+}D^{*-}$  [ $\cos\phi(D_{\text{rec}}^*)$  vs  $\cos\phi(D_{\text{non-rec}}^*)$ ] for the signal region is shown in Fig. 2(a). This two-dimensional distribution is fitted by a sum of three functions corresponding to the  $D_T^*D_T^*$ ,  $D_T^*D_L^*$ , and  $D_L^*D_L^*$  final states,

obtained from the MC simulation. The fit finds  $6^{+15}_{-13}$ ,  $708 \pm 36$ , and  $4^{+18}_{-17}$  events associated with  $D_T^*D_T^*$ ,  $D_T^*D_L^*$ , and  $D_L^*D_L^*$  final states, respectively. Figure 2(b) shows the  $D^{*-}$  meson helicity distribution for  $e^+e^- \rightarrow D^+D^{*-}$ . A fit finds  $433 \pm 24$  and  $-1.5 \pm 2$  events corresponding to  $DD_T^*$  and  $DD_L^*$ , respectively.

We conclude that in  $e^+e^- \rightarrow D^{*+}D^{*-}$  and  $e^+e^- \rightarrow D^+D^{*-}$  production the final states are saturated by  $D_T^*D_L^*$  and  $DD_T^*$ .  $DD_T^*$  is required by angular momentum and parity conservation for  $e^+e^- \rightarrow D^+D^{*-}$  via a virtual photon; the  $D_T^*D_L^*$  result is nontrivial. The production angle distributions for  $e^+e^- \rightarrow D_T^{*+}D_L^{*-}$  and  $e^+e^- \rightarrow D^+D_T^{*-}$  are, therefore, fixed to be  $1 + \cos^2\theta$  in both cases. As a cross check we study the production angle distributions for  $D^{*+}$  from  $e^+e^- \rightarrow D^{*+}D^{*-}$  and  $D^+$  from  $e^+e^- \rightarrow D^+D^{*-}$  processes. After correction for reconstruction efficiency in bins of the production angle, we fit the production angle distributions with the function  $(1 +$

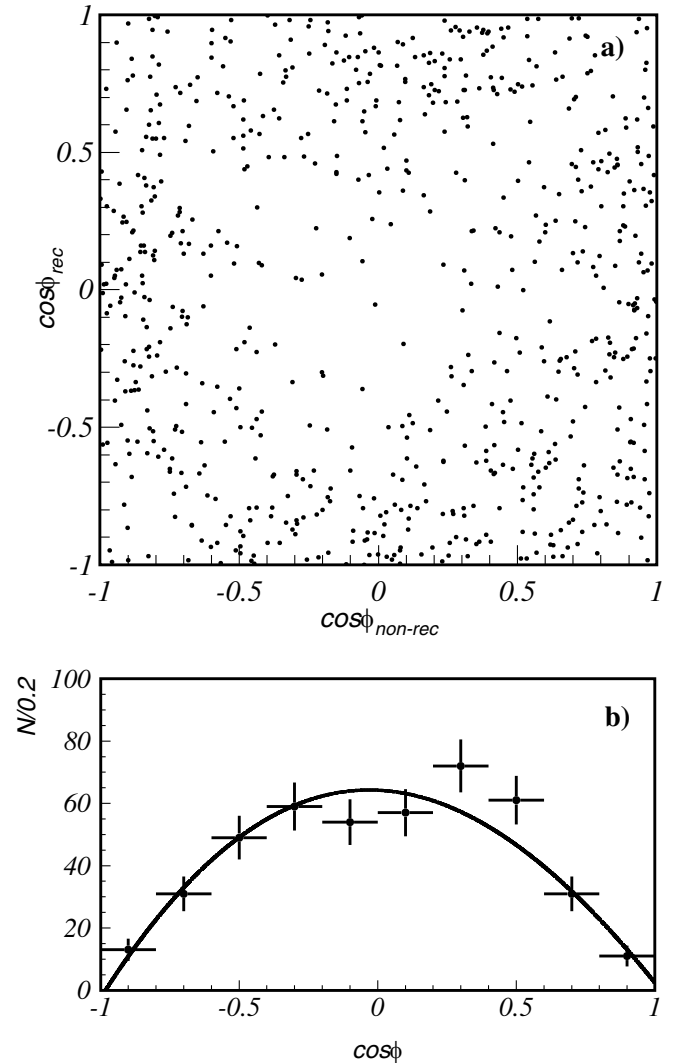


FIG. 2. (a) A scatter plot of  $\cos(\phi_{D_{\text{rec}}^*})$  vs  $\cos(\phi_{D_{\text{non-rec}}^*})$  for  $e^+e^- \rightarrow D^{*+}D^{*-}$  events. (b)  $D^{*-}$  meson helicity angle distribution for  $e^+e^- \rightarrow D^+D^{*-}$  signal candidates. The curve represents the fit described in the text.

$A \cos^2\theta$ ). The parameters  $A$  are found to be equal to  $0.79_{-0.30}^{+0.34}$  and  $2.3_{-0.7}^{+0.8}$  for the two processes, which are in agreement with the expected value  $A = 1$  for both processes.

To calculate the Born cross section for the studied processes, we determine the fraction of events in the signal region with an  $ISR$  photon energy smaller than the chosen cutoff ( $E_{\text{cutoff}} = 10$  MeV) using a MC simulation. In the MC we assume a  $1/q^6$  dependence of the ratio of the cross section to  $\sigma(e^+e^- \rightarrow \mu^+\mu^-)$  as predicted by Ref. [1]. We also try a  $1/q^2$  dependence (corresponding to flat form factors) and include the resulting shift of the event fraction ( $< 1.3\%$ ) in the systematic error. The reconstruction efficiencies are determined from MC simulation. The Born cross sections for  $e^+e^- \rightarrow D^{(*)+}D^{*-}$  are calculated according to the formulas in Ref. [8] and are listed in Table I. The final result is independent of the choice of  $E_{\text{cutoff}}$ . The sources of systematic error are summarized in Table II. The dominant contributions are from the uncertainties in tracking efficiency and  $D^{(*)}$  branching ratios. As the sources of the systematic errors are not correlated, the systematic errors are added in quadrature, negative and positive separately.

We search for the process  $e^+e^- \rightarrow D^+D^-$  by studying the mass spectrum of the system recoiling against the reconstructed  $D^+$  without requiring an extra soft pion in the event. In the  $e^+e^- \rightarrow D^{*+}D^{*-}$  and  $e^+e^- \rightarrow D^+D^{*-}$  analyses, backgrounds are strongly suppressed by the  $\Delta M_{\text{recoil}}$  cut, which is not applicable for the  $e^+e^- \rightarrow D^+D^-$  search; without this requirement the combinatorial non- $D^+$  background is significant. We use  $D^+$  mass sidebands ( $20 \text{ MeV}/c^2 < |M_{K\pi\pi} - M_D| < 35 \text{ MeV}/c^2$ ) to extract the  $M_{\text{recoil}}$  distribution for the combinatorial background. Figure 1(c) shows the  $M_{\text{recoil}}(D^+)$  distribution after  $D^+$  mass sideband subtraction. We fit this distribution with the sum of two signal functions corresponding to  $D^-$  and  $D^{*-}$  peaks and a background function. The latter is a threshold function,  $\alpha[M_{\text{recoil}}(D^+) - M(D^-) - M(\pi^0)]^\beta$ , convolved with the detector resolution, where  $\alpha$  and  $\beta$  are free parameters. For the fit we use only the region  $M_{\text{recoil}} < 2.25 \text{ GeV}/c^2$ , because of a possible contribution of  $e^+e^- \rightarrow D^{(*)}D^{**}$  at higher  $M_{\text{recoil}}$ . The fit finds  $13 \pm 24$  events in the  $D^-$  peak and  $935 \pm 42$  in the  $D^{*-}$  peak. The fit function is shown in Fig. 1(c) as the solid line; the dashed line shows the

TABLE I. The Born cross section results. The first error is statistical and the second one is systematical.

Process	$\sigma_{\text{Born}}$ (pb)
$e^+e^- \rightarrow D_T^{*+}D_T^{*-}$	$< 0.02$ @ 90% C.L.
$e^+e^- \rightarrow D_T^{*+}D_L^{*-}$	$0.55 \pm 0.03 \pm 0.05$
$e^+e^- \rightarrow D_L^{*+}D_L^{*-}$	$< 0.02$ @ 90% C.L.
$e^+e^- \rightarrow D^+D_L^{*-}$	$< 0.006$ @ 90% C.L.
$e^+e^- \rightarrow D^+D_T^{*-}$	$0.62 \pm 0.03 \pm 0.06$
$e^+e^- \rightarrow D^+D^-$	$< 0.04$ @ 90% C.L.

TABLE II. Summary of systematic errors for the  $e^+e^- \rightarrow D^{*+}D^{*-}$  and  $e^+e^- \rightarrow D^+D^{*-}$  measurements.

Source	$e^+e^- \rightarrow D^{*+}D^{*-}$	$e^+e^- \rightarrow D^+D^{*-}$
Tracking efficiency	7%	5%
Identification	2%	2%
Backgrounds	$+0$ $-1.6$ %	$+0$ $-2.5$ %
Form-factor shape	1.3%	1.3%
Luminosity	1%	1%
$\mathcal{B}(D^{(*)})$	4%	8%
Total	9%	10%

contribution of events with  $ISR$  photons of significant energy (larger in this case due to the absence of the  $\Delta M_{\text{recoil}}$  cut); and the dash-dotted line represents the case where the contribution of  $e^+e^- \rightarrow D^+D^-$  is set at the value corresponding to the 90% C.L. upper limit. As the fit finds the background (iii) contribution to be consistent with zero, the dotted line coincides with the horizontal axis. The reconstruction efficiencies for  $e^+e^- \rightarrow D^+D^-$  and  $e^+e^- \rightarrow D^+D^{*-}$  are found from MC. The production angle distribution for  $e^+e^- \rightarrow D^+D^-$  is assumed to be proportional to  $\sin^2\theta$ , while the production angle for  $e^+e^- \rightarrow D^+D^{*-}$  is fixed from the study with the  $\Delta M_{\text{recoil}}$  requirement.

The  $e^+e^- \rightarrow D^+D^{*-}$  Born cross section is calculated to be  $0.54 \pm 0.04$  pb. In this method the systematic uncertainty in the signal yield is larger than in the  $\Delta M_{\text{recoil}}$  method due to significant  $e^+e^- \rightarrow D^+D\pi$  background under the peak, which can be extrapolated only from the higher  $M_{\text{recoil}}$  region with large uncertainties. For the  $e^+e^- \rightarrow D^+D^-$  Born cross section, we set an upper limit of 0.04 pb at the 90% C.L.

The relative sizes of the measured cross sections agree with the predictions of Ref. [1]:  $\sigma(e^+e^- \rightarrow D_T^{*+}D_L^{*-})$  and  $\sigma(e^+e^- \rightarrow D^+D_T^{*-})$  are similar, while  $\sigma(e^+e^- \rightarrow D^+D^-)$  is much smaller.  $e^+e^- \rightarrow D^{*+}D^{*-}$  production is saturated by the  $D_T^{*+}D_L^{*-}$  final state, also as expected. The absolute cross sections are systematically smaller than those of [1] by a factor of 4, which is comparable to the theoretical uncertainty. Recent calculations based on the constituent quark model [3] reproduce the  $D^{*+}D^{*-}$  and  $D^+D^{*-}$  cross sections very well, but predict  $\sigma(e^+e^- \rightarrow D^+D^-) = 0.1$  pb, somewhat larger than our limit. The predicted  $D_L^{*+}D_T^{*-}$  fraction in  $e^+e^- \rightarrow D^{*+}D^{*-}$  production, 65% [3], is smaller than we observe.

In summary, we report the first measurement of the cross sections for the  $e^+e^- \rightarrow D_T^{*+}D_L^{*-}$  and  $e^+e^- \rightarrow D^+D_T^{*-}$  processes at  $\sqrt{s} \simeq 10.6$  GeV and set upper limits on the  $e^+e^- \rightarrow D_T^{*+}D_T^{*-}$ ,  $e^+e^- \rightarrow D_L^{*+}D_L^{*-}$ ,  $e^+e^- \rightarrow D^+D_L^{*-}$ , and  $e^+e^- \rightarrow D^+D^-$  cross sections.

We are grateful to A. G. Grozin for useful discussions and comments on theoretical issues. We thank the KEKB group for the excellent operation of the accelerator, the KEK Cryogenics group for the efficient operation of the solenoid, and the KEK computer group and the NII for

valuable computing and Super-SINET network support. We acknowledge support from MEXT and JSPS (Japan); ARC and DEST (Australia); NSFC (Contract No. 10175071, China); DST (India); the BK21 program

of MOEHRD and the CHEP SRC program of KOSEF (Korea); KBN (Contract No. 2P03B 01324, Poland); MIST (Russia); MESS (Slovenia); NSC and MOE (Taiwan); and DOE (U.S.A.).

- 
- [1] A.G. Grozin and M. Neubert, *Phys. Rev. D* **55**, 272 (1997).
  - [2] A.G. Grozin (private communications).
  - [3] K.-Y. Liu *et al.*, hep-ph/0311364.
  - [4] Charge conjugation and summation over charge conjugated modes are implied throughout the paper.
  - [5] A. Abashian *et al.*, *Nucl. Instrum. Methods Phys. Res., Sect. A* **479**, 117 (2002).
  - [6] S. Kurokawa and E. Kikutani, *Nucl. Instrum. Methods Phys. Res., Sect. A* **499**, 1 (2003).
  - [7] Particle Data Group, K. Hagiwara *et al.*, *Phys. Rev. D* **66**, 010001 (2002).
  - [8] E. A. Kuraev and V.S. Fadin, *Sov. J. Nucl. Phys.* **41**, 466 (1985).